Seventh International Symposium

Machine Processing of Remotely Sensed Data

with special emphasis on

Range, Forest, and Wetlands Assessment

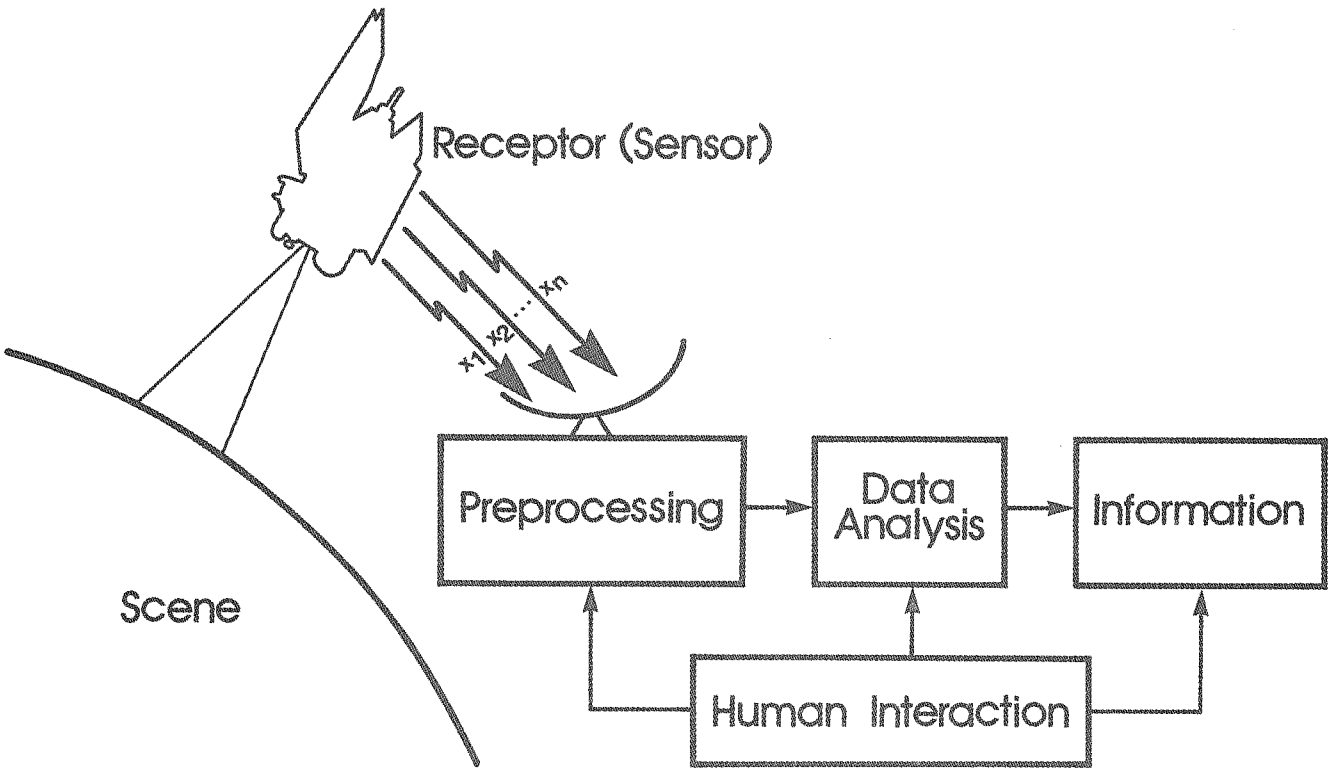

June 23-26, 1981

Reprints From Proceedings

Purdue University
Laboratory for Applications of Remote Sensing
West Lafayette, Indiana 47907 USA

CORRECTING FOR ANISOTROPIC REFLECTANCES IN REMOTELY SENSED IMAGES FROM MOUNTAINOUS TERRAINS *

HEINZ HUGLI, WERNER FREI

Medical Imaging Science Group
University of Southern California
Marina del Rey, California

I. ABSTRACT

Remotely sensed images from mountainous terrains are subject to important radiometric variations which we desire to correct. A quantative analysis of a remote sensing model is presented and the different aspects of radiometric correction are overviewed. A computer simulation is performed in order to better understand the combined effects of anisotropic reflectance characteristics and variable surface orientations, as encountered in remote sensing of mountainous terrains covered with vegetation. The results illustrate typical reflectance effects and show that the possibilities for a radiometrical correction are limited. This is due to the practical difficulty of exactly determining all reflection properties in a mountain environment. However, as a practical approach to the correction, a compensation method is proposed, which considers the particularities of vegetated surfaces in mountainous regions.

II. INTRODUCTION

A. CHANGE DETECTION

Multitemporal remote sensing is used to survey physical and biological processes on the earth surface. Such processes may be analyzed by detecting the change that occur between images taken at different times. Computerized image change detection has several advantages over classical photointerpretation in performing this task[4]. However, a problem of the automatic method is its sensitivity to changes not related to the processes of concern. Such changes result from differences in the recording conditions of subsequent images which include differences in the illumination and the viewing conditions, the characteristics of the atmosphere as well as the pick-up characteristics of the recording devices.

Of course, an ideal situation would be the case where all images of a multitemporal image set are taken under exactly the same conditions. This would result in images differing only by the amount of physical or biological changes occured on the earth surface. Unfortunately, this is not possible in most practical applications, i.e. where the illumination is very different because the images to be compared are taken for example in Summer and in Winter, where the sensor location is different at each flight and where neither the atmospheric nor the pick-up characteristics are constant. A correction of such extraneous effects is therefore needed.

In the frame of the present work however, we will consider exclusively the radiometrical changes resulting from reflectance variations of the ground. Neither atmospheric nor sensor effects are considered here and in the praxis, it is admitted that an additional correction is required for those effects.

Radiometric correction methods have been investigated since the beginning of remote sensing and most efforts have been concerned with the common purpose of improving the accuracy of remote measurements of surface reflection properties like the albedo[3]. We will now describe the problem of a radiometric correction and review at the same time the various results obtained in that field.

B. REFLECTION PROPERTIES

The heart of the present correction problem is the reflectance characteristic

* The research leading to this paper was sponsored by the Department of Energy under contract DE-AS03-76-SF00113.

of the ground. Any correction method uses some a priori knowledge of reflection properties of the surface of concern in order to perform the required correction. Its accuracy is also basically limited by the discrepancy between model and reality.

A diffuse reflection model or Lambert reflector is a good approximation of the average reflectance characteristic of the part of the earth surface not covered with water. For this, but also for its simple mathematical form, this model is used routinely for performing radiometic corrections[14,15]. Alas, if specific surfaces on the ground are considered separately, the diffuse model appears to be only a rough approximation. Excepting those areas covered with loose sand or fresh fallen snow[9], most of the earth surface has anisotropic reflection properties. Water and glazed snow are typical forwardscatters whereas volcanic rocks[6] and plowed fields[2] are typical backscatters.

The typical forwardscatter and the typical backscatter have both their analytical reflection model. Backscattering was analysed extensively in connection with the search for an explanation of the radiometrical behaviour of the moon[10,5]. This studies resulted in a backscatter reflection model which, if it fits better the moon than the earth, gives nevertheless a good insight into the reflection process responsible for backscattering.

The other typical model, the forwardscatter or specular reflection model resulted from measurement on snow and metallic surfaces and is known as the Torrance-Sparrow model[1,16,17].

More complex and less predictable are the reflection properties of vegetated surfaces. Their complexity is the direct consequence of the complexity of the geometrical structure of vegetated surfaces responsible for the reflectance anisotropy. The use of the Duntley equations[13] as a reflection model has been abandoned for a more systematic approach consisting of measuring all reflection properties of all important vegetated canopies likely to be encountered in aerial images[2,8], and building a reflection model which is defined numerically. The advantage of a numerical model is its capability for modeling any complex behaviour. It is a very efficient tool for it can be used as a model of reflection or as a mean of comparing different canopies or also, as a mean of measuring the degree of radiometric homogeneity within a given canopy[7]. Finally a reflection model based on a diffuse surface perturbated by either spheres or cylinders has been analysed and proposed as a practical model for vegetated surfaces[3].

C. HIGH VERSUS LOW ALTITUDE IMAGERY

Because of their particularities, the high altitude or spaceborne imagery and the low altitude or airborne imagery do not give rise to the same difficulty for radiometric corrections. The visual angle under which the images are taken is usually small for high altitude images whereas it is large for low altitude images. Large reflectance variation are therefore produced by the anisotropic characteristic of the ground in low altitude imagery, which is therefore also more difficult to correct. In the past, such important reflectance variations in low altitude imagery of flat regions were either reduced by reducing the visual angle[18], or compensated for their major source of anisotropy which is the hot spot produced by a strong backscattering[11] or corrected according to a complex reflection model[3].

D. FLAT VERSUS MOUNTAINOUS TERRAINS

In all applications and models considered so far, the ground was considered flat. In mountainous terrains, the problem is more complex. Here indeed, the radiometry is the consequence of the combined effect of reflection properties and surface orientation. The radiometric correction method for flat regions must therefore be modified to account also for the spatially varying surface orientation.

An approach to this problem is to consider the ground as a curved surface with defined reflection properties. The theoretical ground reflectance can thus be computed using both a given reflection model like the one above and a geometric model as a description of the surface. Radiometric corrections can be performed on this basis. This was done previously using a diffuse reflectance characteristic and a digital terrain model to account for the relief[15].

The question arises, wether this approach can be generalized for the reflectance characteristics of natural surfaces which are anisotropic. We shall analyse this question and simulate the practical effect resulting from this generalisation. Then, we compare this synthetic images with real photographic images in order to illustrate the utility of using an anisotropic reflectance model.

A different and even more general approach consisting of an orientation dependent reflectance characteristic will then be analysed. We shall show that with it, we reach the limits of a practical modeling of the ground.

II. REMOTE SENSING MODEL

For the purpose of the present analysis, a remote sensing model is set up and used as a mean to analyse the reflection mechanisms on the earth surface. The earth surface is illuminated by natural light on one hand and viewed by a light sensing system on the other hand (figure 1). Light from the source falls on a ground surface element or target which then reflects part of it toward the sensor. The illumination of the target has two basic components: direct sunlight and spatially distributed skylight. The direct sunlight is a collimated beam of irradiance Eo. Because of foreshortening, the irradiance on the target produced by the direct beam is reduced to:

$$Ei = Eo \cdot \cos(Ti)$$

where Ti is the beam incidence angle on the target.

The spatially distributed skylight can be characterized by a radiance function Li'(Ti,Fi) which defines how much light the target receives from each sky direction. For more simplicity in this paper, the skylight will be ignored. However this approach is valid only partially, it has the merit to show the nature of the correction problem.

Then, the irradiated target reflects light in the whole hemisphere. The radiance Lr in the direction of the sensor depends on the target reflection properties and the geometry of the incident and reflected beams. It is fully described by the bidirectional reflectance distribution function (BRDF) which is denoted by the symbol fr and defined as the ratio of reflected radiance dLr in the direction of the sensor to the irradiance dEi in the direction toward the source:

$$fr(Ti,Fi,Tr,Fr) = dLr(Ti,Fi,Tr,Fr) \,/\, dEi(Ti,Fi)$$

where Ti and Tr, respectively Fi and Fr are the spherical angles of the incident, respectively reflected beams in the target hemispherical coordinate system T,F (figure 2). The radiance of a target with a given BRDF can thus be computed according to:

$$Lr = \int_{\Omega} fr \cdot dEi$$

where Ω refers to the whole hemispherical solid angle for the reflection.

III. GEOMETRY OF THE TARGET

Figure 1 shows the target as an element of the earth surface E(X,Y) within the basic coordinate system X,Y,Z defined by the directions East, North and Zenith respectively. The vector $\underline{n}^*$ normal to the target is obtained from the surface E(X,Y) with:

$$\underline{n}^* = (-dE(X,Y)/dX,\ -dE(X,Y)/dY,\ 1)$$

The direction of the illumination source is given by $\underline{i}^*$ = (Ix, Iy, Iz) and that of the viewer is obtained from the viewer location (Vx, Vy, Vz) by:

$$\underline{r}^* = (\ Vx-X,\ Vy-Y,\ Vz-Z\ )$$

The unit vectors $\underline{n}$, $\underline{i}$ and $\underline{r}$ are obtained by normalizing $\underline{n}^*$, $\underline{i}^*$ and $\underline{r}^*$ respectively.

An other important direction which will be used later is that of the highlight unit vector h which lies halfway between $\underline{i}$ and $\underline{r}$. Computationally:

$$\underline{h} = (\underline{i}+\underline{r}) \,/\, |(\underline{i}+\underline{r})|$$

Obviously the highlight direction is constant for constant $\underline{i}$ and $\underline{r}$. We can think of it as the direction resulting from $\underline{i}$ and $\underline{r}$ which the target normal must have in order to produce usually the maximum of specular reflection.

So far, these vectors are specified in the rectangular coordinate system X,Y,Z bound to the terrain. To perform the reflectance computation, their spherical coordinates in the target system (figure 2) are needed. As coordinates we will use here the cosinus of the spherical angles which we decide to call the M-variables. They are as follows:

- The incidence angle Ti:

$$Mi = \cos(Ti) = \underline{n} \cdot \underline{i}$$

- The reflection angle Tr:

$$Mr = \cos(Tr) = \underline{n} \cdot \underline{r}$$

- The phase angle Ap:

$$Mp = \cos(Ap) = \underline{i} \cdot \underline{r}$$

- The half phase angle Aq = Ap/2:

$$Mq = \cos(Aq) = \underline{i} \cdot \underline{h} = \underline{r} \cdot \underline{h}$$

- The azimuthal angle F between $\underline{i}$ and $\underline{r}$, which is derived by using the cosinus law for the spherical triangle Ti, Tr and Ap. We have:

$$Mf = \cos(F)$$

$$Mf = \frac{\cos(Ap) - \cos(Ti).\cos(Tr)}{\sin(Ti).\sin(Tr)}$$

- The off-specular angle As, finally:

$$Ms = \cos(As) = \underline{n} \cdot \underline{h}$$

IV. REFLECTION MODELS

The reflection properties are fully described by the BRDF which is therefore an ideal tool for comparing different reflection models. Choosing a reflection model is identical to choosing a BRDF. The BRDF can be defined either analytically or numerically.

A. DIFFUSE MODEL

An ideal diffuser has a constant radiance Lr and reflects all incident light. Consequently, its BRDF is constant and its value is:

$$fr,id = const$$

A real diffuser has a constant radiance Lr and, because of absorption, reflects the fractional part Ro of all the incident light. The value of its BRDF is:

$$fr,d = const \cdot Ro$$

B. TORRANCE-SPARROW'S SPECULAR MODEL

This model has shown to be very close to the reflection characteristic of shiny surfaces. For its quality, it has become a usefull tool for computer graphics . Its BRDF is modeled as being composed of a diffuse and a specular component, that is:

$$fr,ts = Ks \cdot S + Kd$$

where Ks and Kd are model parameters defining the diffuse and specular proportions respectively, and S is the specular function. This function is given by:

$$S = \frac{D(Ms).F(Mq,ni).G(Ms,Mr,Mi,Mq)}{Mi.Mr}$$

when expressed with the M-variables. The functions D, F and G are as follows. D is the microfacet distribution function which is typically

$$D(Ms) = Ms^{Ke}$$

where Ke is a model parameter permitting to specify the width of the specular hightlight peak.

F is the Fresnel reflection function for the beam falling on a microfacet with a refraction index ni, under the angle of incidence Aq = arccos(Mq). Its value is:

$$F(Mq,ni) = \frac{1}{2}\left(\frac{W}{V}\right)^2\left(1 + \left(\frac{Mq.V-1}{Mq.W+1}\right)^2\right)$$

where:

$$W = \sqrt{ni^2 + Mq^2 - 1} - Mq$$

$$V = \sqrt{ni^2 + Mq^2 - 1} + Mq$$

Finally G is an attenuation factor considering the shadowing effects appearing at large incidence angles Ti and large reflection angles Tr. Its value is:

$$G(Mi,Mr,Ms,Mq) = \min(\ 1,\ 2.Mr.Ms/Mq,\ 2.Mi.Ms/Mq\ )$$

This concludes the description of the Torrance-Sparrow BRDF as a function of the M-variables. The model itself is dependent on the model parameters Ks and Kd, the exponent Ke defining the specular peak width and the refraction index ni.

C. HAPKE'S BACKSCATTERING MODEL

This model was especially developped to fit the BRDF of the moon which is characterized by strong backscattering. Its BRDF is given by the expression:

$$fr,h = Kh \cdot fr,l(Mi,Mr) \cdot B(Ap) \cdot Z(Ap)$$

where Kh is a scaling coefficient and the functions fr,l, B and Z are as follows: fr, l is the BRDF of the Lommel-Seelinger reflection law[10], whose expression is:

$$fr,l(\ Mi,\ Mr) = 1\ /\ (1 + Mr/Mi)$$

Its value does not vary much from 0.5 for a small incidence angle Ti and reflection angle Tr and its main merit in the Hapke's expression is to let the function become zero when Ti is $\pi/2$.

Then, B is the retrodirective function responsible for the backscattering. Its form is:

$$B(Ap) = \begin{cases} 1 & \text{if } Ap >= \pi/2 \\ 2 - \frac{1}{2t}\left(1-e^{-t}\right)\left(3-e^{-t}\right) & \text{else} \end{cases}$$

where t= Kg / tg(Ap)

The parameter Kg is a mean to control the width of the backscattering peak and is therefore also a model parameter.

Finally, the function Z is the scattering law of the surface. It is used as a mean of changing the relative importance of forwardscattering and backwardscattering. It has three distinct forms but only under its form for increased backscattering does it have a real physical justification. It is written as:

$$Z(Ap) = \frac{\sin(Ap) + (\pi - Ap).\cos(Ap)}{\pi}$$

To conclude, Hapke's BRDF is a function of the three variables Mi,Mr and Ap. It is also dependent on the model parameters Kh and Kg. These parameters are means for fitting the model to the reality.

D. EGBERT'S MODEL

In this model, a ground plane is being considered covered with either spherical or cylindrical perturbations. The surface of both the plane and the perturbations is supposed to be a Torrance-Sparrow reflector, i.e. to have a combined diffuse and specular reflection. Thus, the BRDF of Egbert's model is as sum of five terms which are: the diffuse and specular parts of both the plane and the perturbations, and the diffuse part of the shadows. The proportion of each term is fixed by coefficients which were experimentally shown to be essentially dependent on two parameters only: the density of the perturbations and their size.

E. NUMERICAL BRDF

Extensive measurements of natural surfaces have been done [2,5,7,8] which can be used as numerical BRDF. The exact measurement of the BRDF of a given surface is a tedious work because the BRDF is a function of 4 variables. Indeed, the measurement of a BRDF based on a spherical raster grid with a mesh of 10 degres both on the incidence and on the reflection hemispheres, requires for instance (36*8)**2 = 82944 single measurements. This number is reduced to its half using the reciprocity propriety of the BRDF[12]:

fr(Ti,Fi,Tr,Fr) = fr(Tr,Fr,Ti,Fi)

This number is further significantly reduced by reducing the number of variables to 3, assuming the rotational symetry of the target:

fr,4(Ti,Fi,Tr,Fr) = fr,3(Ti,Tr,F)
where F = abs(Fi - Fr)

Such an assumption is reasonable for most natural surfaces. Under these circumstances, the number in the above example is reduced to (8*8*19) = 1216 which is the number of single measurements to perform for measuring the BRDF of a single target. It gives also the storage requirement for using it in a computer simulation. This number must be multiplied by the number of channels in multispectral applications.

V. FOUR MODELS COMPARED

In order to better understand their anisotropic behaviour, we compare the shape of different reflection models. We choose to compare the shape of both the bidirectional reflectance distribution function (BRDF) and the bidirectional reflectance (BR) because both are commonly used. The BRDF has yet been defined as the ratio of the reflected radiance dLr toward the sensor to the irradiance dEi toward the source:

BRDF= fr(Ti,Fi,Tr,Fr)
BRDF= dLr(Ti,Fi,Tr,Fr) / dEi(Ti,Fi)

Similarly, the BR is defined as the ratio of the flux dXr reflected toward the sensor to the flux dXo emitted by the source toward the target:

BR= R(Ti,Fi,Tr,Fr)
BR= dXr(Ti,Fi,Tr,Fr) / dXo(Ti,Fi)

We are not interested here in the absolute values of this reflectances but in their shape and thus consider them scaled arbitrary. Under this assumption, R and fr are related by:

R = fr . cos(Ti)

The behaviour of four typical surfaces, namely sand, lunar surface, glazy snow and forest is now compared. The corresponding models as well as the parameters are summerized in table A. These models all use the rotational invariance of the surface so their BRDF and BR are functions of 3 variables. Their representation is as follows.

The figures 4 and 5 show the BRDF respectively the BR of the four surfaces in the plane of incidence (Fi= 0 and 180 degrees) as a function of the angle of reflection Tr for several angles of incidence. These figures illustrate the strong anisotropies we are expected to make a correction for.

VI. VISUAL SIMULATION

We simulate now the remote sensing process and generate synthetic views to illustrate the combined effect of isotropic reflectances and mountainous terrains. The

required elements for the generation are basically a digital terrain model to account for the relief and a reflection model like one of the models described above.

The digital terrain model presently used is derived from the USGS data set[19]. It covers the site of Redondo Peak, New Mexico with a size of 15.5 km * 15.5 km and consists of 256 * 256 elevation elements equally spaced on a rectangular grid. As reflection models, we will consider the four models previously described which respectively stand for sand, moon, snow and forest.

The question arises how to combine terrain model and reflection model. The present simulation is based on the assumption that the reflection model of the surface spanning the model is constant, i.e. it is both space and slope invariant. This assumption is the key to the generation of synthetic views which then comprises the following steps: a) defining the light source vector $\underline{i}$ which is constant for the whole image; b) using the location of the sensor and the digital terrain model to determine pixel by pixel the value of the directions $\underline{n}$ and $\underline{r}$; c) transforming $\underline{i}$, $\underline{n}$ and $\underline{r}$ in M-variables and finally d) computing the image luminance according to the four different reflection models.

Figure 6 shows the results of the simulation. Shown are vertical views on both a flat and a mountainous site which reflect light according to the four reflection models sand, moon, snow and forest. The sensor or viewer is located on different images at different distances from the ground and the viewing angle is adjusted in order to maintain visible the same part of the site. In figure 6a the mountainous terrain is viewed from a geostationary orbit under a viewing angle of 0.02 degrees. The sites of both figures 6b and 6c are viewed from the same altitude of 25,000 feet. In order to make the comparison between both images 6b and 6c easy, the 8000 feet altitude of the flat site was choosen to fit the mean altitude of the mountainous terrain. We also use this mean altitude to determine the viewing angle which value is then 112 degrees. As for the figure 6d, this is an extreme case where the site is viewed from an altitude of 15,000 feet which results in a mean viewing angle of 145 degrees.

The main thing shown by these images is the effect of anisotropic BRDF on the overall radiometry of the resulting images. The isotropic sand model is used here as a reference and its images are of course unchanged in the different views. The moon model gives rise to a very strong hot spot whose location, as expected, is different in each image. The snow model also illustrates the typical effect of shiny surfaces on the image radiometry with its typical specular spots or highlights dependent on the terrain orientation. Finally the forest models also produces important radiometric changes in the images which are however less easy to interpret.

The images resulting from the numerical forest model suggest the following comments. First, the image of the flat site reveals a rough quantization of the numerical BRDF. Although the values are computed from the numerical BRDF by mean of a trilinear interpolation, important radiometric variations are visible which suggest that a more accurate model is needed if radiometric corrections are to be performed on this basis.

Second, looking nearer at the forest images of figures 6a, c and d reveals an important increase in the overall luminance when the viewer distance to the ground increases. This is well explained by the corresponding increase of the reflection angles of the single pixels. An other visible effect is the strong luminance variation as a function of the surface orientation in the mountainous terrain. This variation is in fact much more important for the forest than the corresponding variation in the case of the diffuse model. We have to explain this phenomena which does not correspond to what we really see on images from forest in mountainous terrains. A pertinent explanation is that the basic assumption we made for this simulation is not valid. This would also mean that a different description of the reflection is required in mountainous terrains.

VII. GENERALIZED MODEL

A. GENERALIZATION

The results of the simulation suggest that at least for the forest model the assumption of an orientation invariant surface spanned on the relief does not hold. This suggestion will now be reinforced by the following explanation of the real meaning of this assumption.

Let us consider a surface covered with forest. In the case of a flat site as shown in figure 3a, the BRDF is:

$$fr = fr(\, Ti, Tr, F \,)$$

where:

$$Ti = \text{const}$$
$$Tr = Tr(\, X, Y)$$
$$F = F(\, X, Y)$$

The case of the mountainous site where the assumption of a constant BRDF is made is shown in figure 3b and is described by the following orientation invariant BRDF:

$$fr = fr(\, Ti, Tr, F)$$
where:
$$Ti = Ti(\, dE/dX, dE/dY)$$
$$Tr = Tr(\, X, Y, dE/dX, dE/dY)$$
$$F = F\,(\, X, Y, dE/dX, dE/dY)$$

The invariance assumed in this case supposes trees growing perpendicularly to the tilted surface which is obviouly not the case in the reality. Hence, this explains the phenomena observed before on the images and suggests also that such a model is unable to describe the exact behaviour of vegetated surfaces with variable orientation.

A more general model is thus required to describe the reflection of the surface of figure 3c. An orientation dependent BRDF makes this possible:

$$fr = fr(\, Ti, Tr, F, dE/dX, dE/dY\,)$$
where Ti, Tr and F are as above.

B. PRACTICAL LIMITS OF REFLECTION MODELING

With a five variable BRDF like the above we reach the reasonable practical limits of the reflection modeling. This is particularly the case when working with numerical BRDFs in which case the determination of the model alone would require a prohibitive amount of measurements. But this is also true if an analytical BRDF is used (assumed such a model can be found), because here also, its determination would be a very tedious measurement process.

Above all, it is doubtfull that a such very precise model can really be used. This is because the vegetated surfaces in mountainous terrains lack the relative homogeneity encountered on some flat sites and that a very precise model is therefore not worth while.

VIII. PRACTICAL CORRECTION METHOD

We will now treat a more practical approach of the radiometric correction of remote sensed images. Because of the above mentionned difficulty to define an exact model of reflection we will concentrate on the correction of the major radiometric inhomogeneities in the image.

In remote sensed images from mountainous terrains, the most obvious radiometric variations which are caused by illumination and viewing effects are the consequence of a) forshortening and b) backscattering. Forshortening describes the variation of the effective surface of the target when its orientation is changed and is considered by the diffuse reflection model. Backscattering is obvious on vegetated surfaces. Even if it is less strong, it is similar to the backscattering of the lunar surface.

These considerations allow us to propose the following practical BRDF built on the BRDFs of both the diffuse model (fr, d) and Hapke's model (fr,h):

$$fr = Kd'.\ fr,d \ + \ Kh\ .\ fr,h$$

or:

$$fr = Kd \ + \ Kh\ .\ fr,h$$

where Kd and Kh are scaling parameters. Their value must be adjusted in order to obtain a best fit between the real recorded image and the synthetic correction image generated with this rule and using the appropriate digital terrain model.

IX. CONCLUSION

We have shown the mechanisms of reflection in the case of natural surfaces in mountainous terrains as well as their effect on the radiometry of remote sensed images. Using the reflectance characteristics of sand, lunar surface, snow and forest, simulated images of mountainous terrains were generated based on the assumption of a surface with an orientation invariant reflectance characteristic. This approach was shown to be feasible only for a certain class of surfaces. Surfaces with an important vertical structure like vegetated surfaces and especially forest require a more complex reflection model which is also a function of the surface orientation. For practical purposes however, a more simple reflection model is proposed which performs the major radiometric corrections of remote sensed images from mountainous terrains.

X. REFERENCES

1. Blinn J.F., 'Models of Light Reflection for Computer Synthesized Pictures', Computer Graphics, Vol. 11, Summer 1977, p. 192-198

2. Eaton F.D. and Dirmhin I., 'Reflected Irradiance Indicatrices of Natural Surfaces and their Effect on Albedo', Applied Optics, Vol. 18, No. 7, 1 April 1979, p. 994-1008

3. Egbert D.D., 'A Practical Method for Correcting Bidirectional Reflectance Variations', Machine Processing of Remotely Sensed Data Symposium, 1977, p. 178-189

4. Frei W., Singh M. and Shibata T., 'Digital Image Change Detection', SPIE Optical Engineering, Mayjune 1980, Vol. 19 Nr. 3, p. 331-338

5. Hapke B.W., 'A Theoretical Photometric Function for the Lunar Surface', Journal of Geophysical Research, Vol. 68, No. 15, August 1, 1963, p. 4571-4586

6. Hapke B. and Van Horn H., 'Photometric Studies of Complex Surfaces, with Applications to the Moon', Journal of Geophysical Research, Vol. 68, No. 15, August 1, 1963, p. 4545-4570

7. Kimes D.S., Smith J.A. and Ranson, 'Vegetation Reflectance Measurements as a Function of Solar Zenith Angle', Photogrammetric Engineering and Remote Sensing, Vol. 46, No. 12, Dec. 1980, p. 1563-1573

8. Kriebel K.T., 'Measured Spectral Bidirectional Reflection Properties of Four Vegetated Surfaces', Applied Optics, Vol. 17, No. 2, 15 January 1978, p. 253-259

9. Middleton W.E.K. and Mungall A.G., 'The Luminous Directional Reflectance of Snow', Journal Optical Society of America, Vol. 42, No. 8, p. 572-579

10. Minnaert M., 'Photometry of the Moon', in 'The Solar System, III, Planets and Sattelites' by Kniper G.P. and Middlehurst B.M., Chicago 1961, p. 213-248

11. Nagao Makoto, 'Low Level Processing for Aerial Photograph Analysis', U.S.-Japan Seminar on Robot Vision, Cambridge Mass., Aug. 1977

12. Nicodemus F.E., Richmond J.C. and Hsia J. J., 'Geometrical Considerations and Nomenclature for Reflectance', National Bureau of Standarts, Monograph 160

13. Reeves R.G., Abraham A. and Landen D., 'Manual of Remote Sensing', American Society of Photogrammetry, Falls Church, Virginia, 1975

14. Robinove Ch.J. and Chavez P.S. Jr., 'Landsat Albedo Monitoring Method for an Arid Region', AAAS Int. Symp. on Arid Region Plant Resources, Lubbock, Texas, Oct. 1978

15. Sjoberg R.W., Horn B.K.P., 'Atmospheric Modelling for the Generation of Albedo Images', Proc. Image Understanding Workshop, DARPA, Maryland, April 30, 1980

16. Torrance K.E. and Sparrow E.M., 'Theory for Off-Specular Reflection from Roughened Surfaces', Journal Optical Society of America, Vol. 57, NO. 9, Sept. 1967, p. 1105-1114

17. Trowbridge T.S. and Reitz K.P., 'Average Irregularity Representation of a Rough Surface for Ray Reflection', Journal Optical Society of America, Vol. 65, No. 5, p. 531-536

18. Walker J.E., 'Photometry: Linking Earth, Air and Analysis', Optical Spectra, August 1979, Vol. 13, Issue 8

19. USGS, 'Digital Terrain Tapes: User Guide', National Cartographic

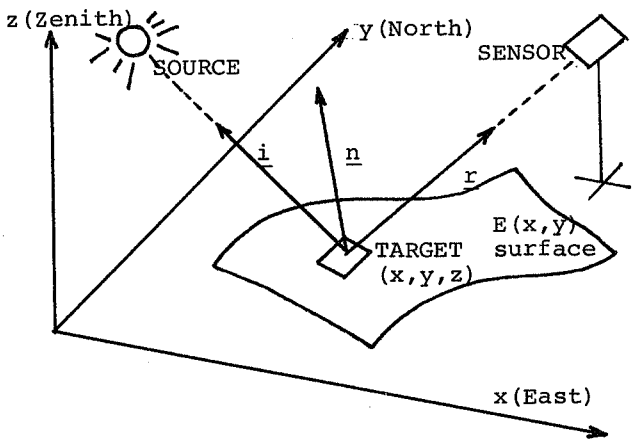

Figure 1. Ground coordinate system with source, target and sensor

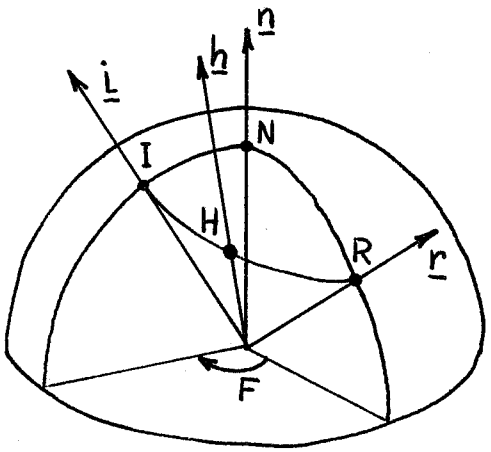

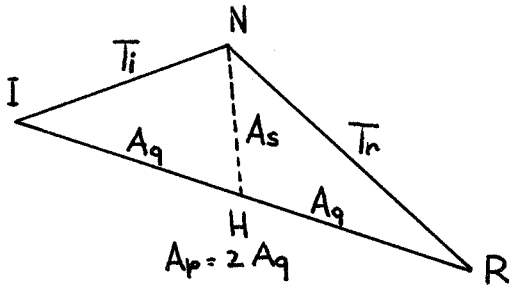

Figure 2. Spherical coordinate system bound to the target

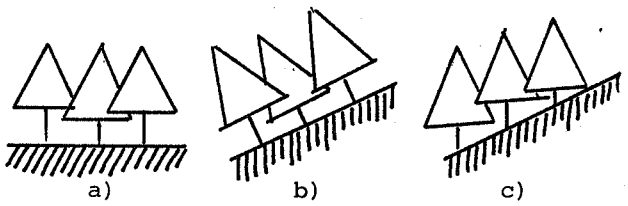

Figure 3. Assumed structure of the ground for different reflection models

	SAND	MOON	SNOW	FOREST
Description:	diffuse surface surface	lunar surface surface	glazed snow	coniferous forest forest (= 580 nm)
Model:	diffuse	Hapke's	Torrance-Sparrow	numerical
Parameters:	fr,d= .6	Kg= .5	Kd= .6, Ks= 30 ni=1.31, Ke=500	from

Table A. Characterization of the four surfaces used in the simulation

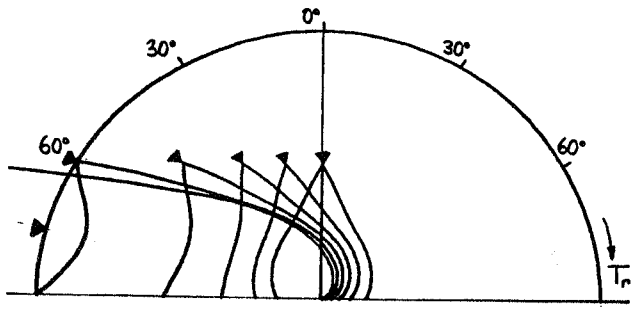

4a) moon

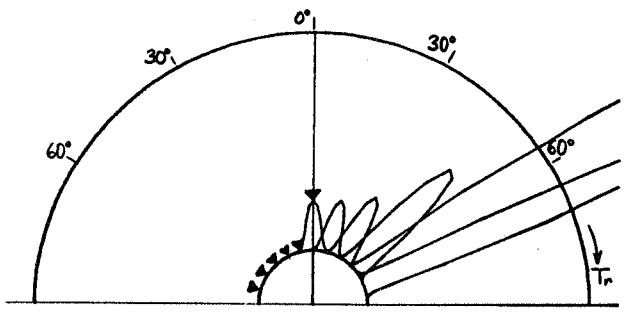

4b) snow

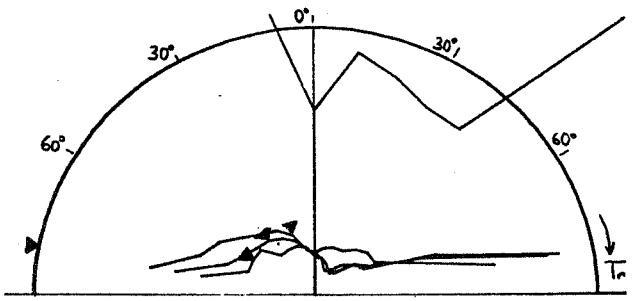

4c) forest

Figure 4. BRDF's of several surfaces shown in the plane of incidence (F=0 and 180 degrees) as a function of the reflection angle Tr. Each curve corresponds to a different angle of incidence Ti marked by an arrow

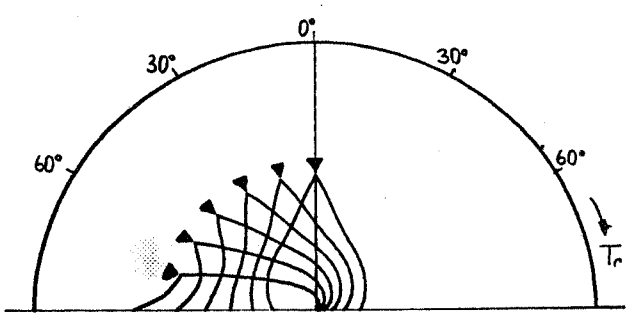

5a) moon

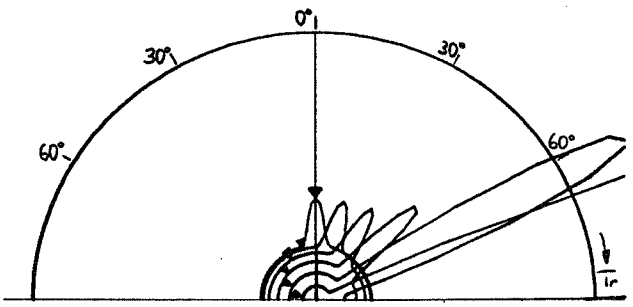

5b) snow

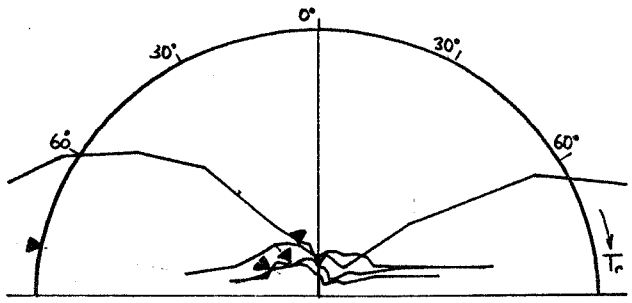

5c) forest

Figure 5. BR's of several surfaces shown in the plane of incidence (F=0 and 180 degrees) as a function of the reflection angle Tr. Each curve corresponds to a different angle of incidence Ti marked by an arrow

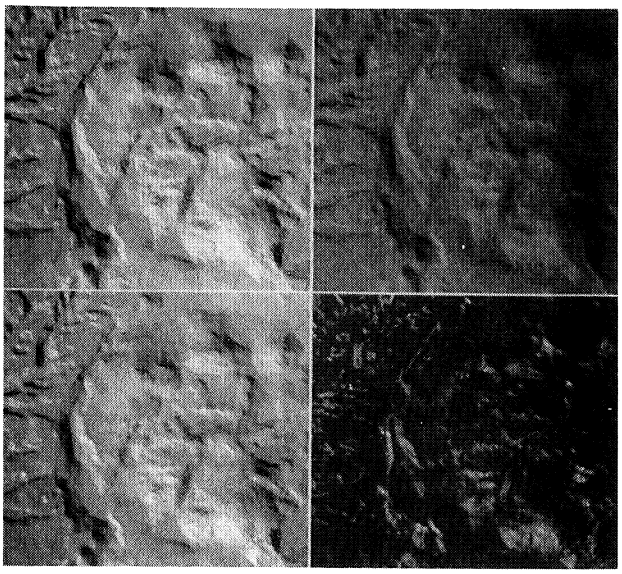

6a)
Mountainous terrain (Redondo Peak) as it is viewed from the space (altitude infinite)

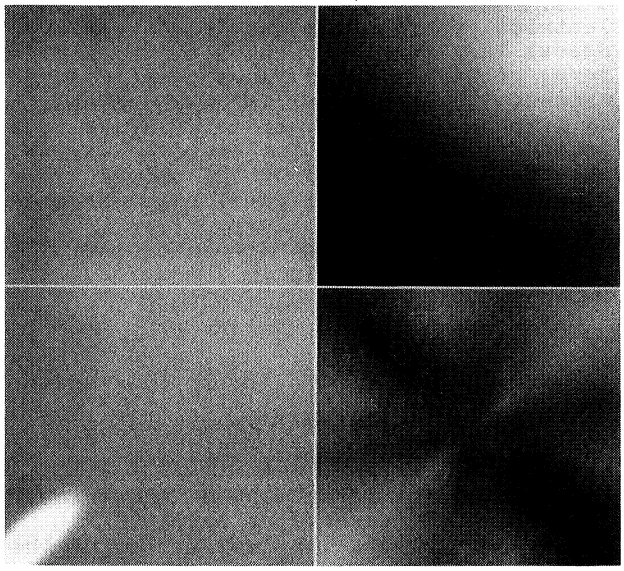

6b)
Flat terrain at an elevation of 8,000 feet as it is viewed from an altitude of 25,000 feet

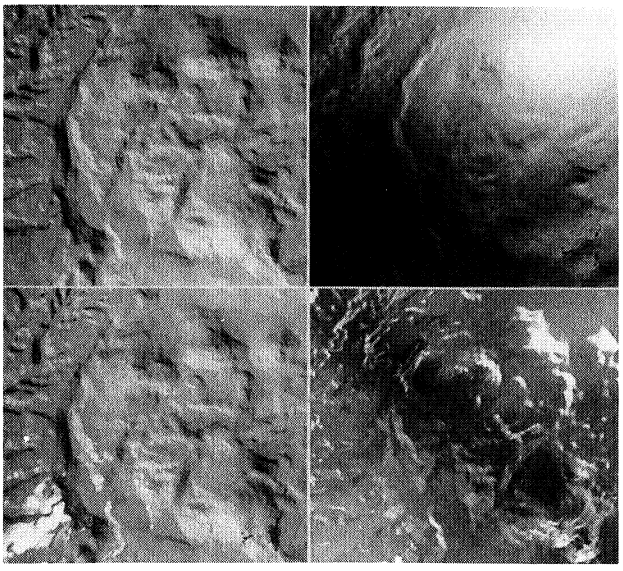

6c)
Mountainous terrain (Redondo Peak) as it is viewed from an altitude of 25,000 feet

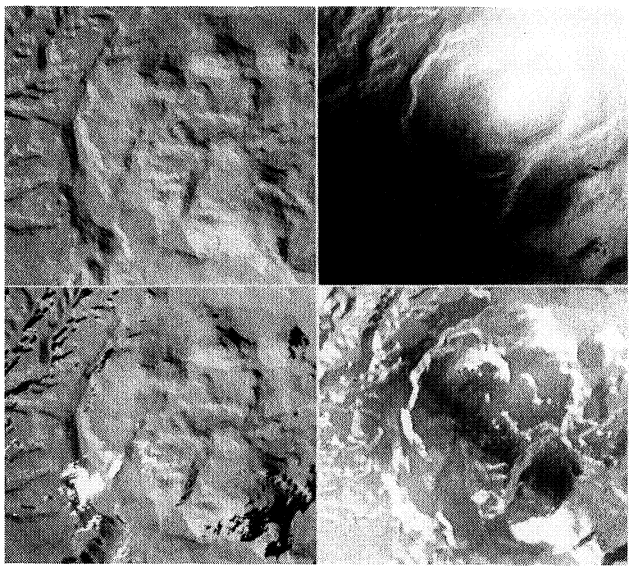

6d)
Mountainous terrain (Redondo Peak) as it is viewed from an altitude of 15,000 feet

Figure 6. Simulated views of a flat and a mountainous terrain according to four different reflection models. North is on top. The illumination is constant and is from South-West at an incidence angle of Ti= 55 degrees.

SAND	MOON
SNOW	FOREST

Heinz Hugli received the B.S. degree in 1971 and the Ph.D. degree in 1980 in electrical engineering from the Swiss Federal Institute of Technology, Zurich. There, he worked for 6 years as a research engineer and consultant in image processing and computer graphics. Since 1980, he is a visiting scientist at the Medical Imaging Science Group, Medical School at the University of Southern California where his research activities include presently remote sensing, computer graphics and medical image processing.

Werner Frei received the B.S. in 1968 and the Ph.D. degree in 1972 in electrical engineering from the Federal Institute of Technology, Zurich, Switzerland. He then became an Assistant Professor at the Department of Electrical Engineering, University of Southern California, Los Angeles, and member of the staff at the USC Image Processing Institute. In 1976, he joined the faculty of the USC Medical School, where he is now Associate Director of the Medical Imaging Science Group of the Department of Radiology. He is in charge of the digital image analysis research effort by the group.